A MODEL OF THE BACK LIT THYRATRON

BY

HOYOUNG PAK

B.S., University of Illinois, 1987

THESIS

Submitted in partial fulfillment of the requirements
for the degree of Master of Science in Electrical Engineering
in the Graduate College of the
University of Illinois at Urbana-Champaign, 1988

Urbana, Illinois

UNIVERSITY OF ILLINOIS AT URBANA-CHAMPAIGN

THE GRADUATE COLLEGE

MAY 1988

WE HEREBY RECOMMEND THAT THE THESIS BY

HOYOUNG PAK

ENTITLED A MODEL OF THE BACK LIT THYRATRON

BE ACCEPTED IN PARTIAL FULFILLMENT OF THE REQUIREMENTS FOR

THE DEGREE OF MASTER OF SCIENCE

Mark Jay Kushner
Director of Thesis Research

Timothy M. Cahill
Head of Department

Committee on Final Examination†

Chairperson

† Required for doctor's degree but not for master's.

O-517

ACKNOWLEDGEMENTS

The author would like to acknowledge the Los Alamos National Laboratory, particularly Dr. Glen McDuff, for their support of this project. He would also like to thank Dr. Martin Gundersen, a professor at the University of Southern California, for his comments and notes on the back lit thyratron.

The author would like to thank his advisor, Professor Mark Kushner, for his patience and guidance throughout the program. He would also like to thank the members of the Gaseous Electronics Laboratory, particularly Tom Moratz, Tim Peck, Mike McCaughey, John Dicarlo, and "gas house" graduate, Todd Saunders, for giving the laboratory a comfortable atmosphere.

The author would like to extend a special thanks to his parents for the support and encouragement they have given him throughout his life. He also thanks his siblings, Cheryl and Hosung, for their friendship.

TABLE OF CONTENTS

I. INTRODUCTION

In recent years there has been an increase in demand to upgrade or replace "conventional" high-powered switching devices, such as thyratrons and spark gaps. High-powered switches are an important component of devices such as lasers, power modulators, and rail guns. Desirable characteristics of their switching devices are high hold-off voltage, fast switching speed, high current density, fast current rise time, minimal jitter, low inductance and long lifetime.

High hold-off voltage is neccesary because many devices are charged over long periods (microseconds) while switched over short times (nanoseconds). High current density is important for our switching device to be reasonable in size, which is as small as possible. From the relationship, $I = J \cdot \text{Area}$, current density is inversely proportional to area. Therefore, higher current densities allow the use of smaller devices without compromising on the output current. From the current-voltage relationship, $V = L \frac{dI}{dt}$, the time rate of change of current is inversely proportional to inductance. Therefore, to achieve fast current rise time, a low value of inductance (i.e., small size) is desired. Even with all parameters held constant, the switch closure time will vary slightly for each trial. The variation of closure time is known as jitter. It is desirable to have minimal jitter so that for a given set of parameters the closure time can be determined accurately.

As a result of the increase in demand for "better" switches, a new class of switching devices has been developed. Two of the newly developed switches are the pseudo-spark and the Back Lit Thyratron, BLT[1-5]. The BLT and the

pseudo-spark are based on similar principles with the major difference being the triggering mechanism. The BLT is optically triggered; the pseudo-spark is electrically triggered. The goals of this thesis are to study the behavior of the BLT and to analyse the conditions that result in optimal performance. This study was performed by constructing a two-dimensional time-dependent computer model for a BLT. The model includes the conservation equations for electrons and ions, secondary emission processes, electron and ion transport, photon transport, and an external electrical circuit. The parameters of interest are gas pressure, gas composition, geometry, open circuit voltage, and duration and amplitude of photon flux from the light source. By observing the changes in performance of the BLT as the various parameters are changed, optimal operating conditions can be determined.

A switching device goes through three distinct states of operation. Initially it is in the open state and all of the source voltage is dropped across the switching device. Triggering the switching device causes it to make a transition to a commutation or switching state. In this stage, current begins to increase and impedance across the switching device begins to collapse. This leads to the final stage, conduction or the closed state. In this state the impedance across the switching device is negligible, causing the switch to behave nearly as a short circuit. This thesis is devoted largely to the analysis of the commutation stage of the Back Lit Thyratron with brief mention of the open and conduction stages.

Extensive research has been done on several switching devices, among the most common are thyratrons and spark gaps. Thyratrons have several disadvantages. Thyratrons use a hot cathode as the current source. This

requires an auxiliary heater, which is cumbersome and may prevent the switch from being electrically isolated. The thyratron geometry is also somewhat cumbersome. In addition to the cathode and anode, there are a control grid, baffle, and auxiliary grid. The control grid separates the anode from the cathode except in a small region where current flows through. The baffle is placed close to the hole in the control grid. Its purpose is to block penetration of high electric fields into the cathode grid region. A major disadvantage of the thyratron is that there is a compromise between hold-off voltage and switching speed resulting from this geometry. For example, a tight baffle leads to a high hold-off voltage, but switching speed is poor. On the other hand, a loose baffle leads to fast switching, but hold-off voltage is poor[6]. The combination of these and several other details makes the thyratron an unattractive switching device, though at present it is the only commercially available device to meet switching requirements. Spark gaps, on the other hand, have a relatively simple geometry, consisting of only an anode and a cathode. However, they also have major disadvantages. Spark gaps cannot be operated at high repetition rates. Spark gaps are triggered by an auxiliary grid or a focused laser aimed at the side of the cathode that faces the anode. The switching mechanism may cause damage to the cathode, resulting in a shorter lifetime of the device.

A relatively new switching device, the BLT (back lit thyratron), takes advantage of many of the positive features of the two switches mentioned above. The BLT, which is an optically triggered version of the pseudo spark, has a simple geometry. It consists of an inverted cup cathode with a central hole to allow transfer of electrons to the anode (Fig. 1). (All figures

precede the references.) The triggering mechanism is one that does not cause degradation to the side of the cathode facing the anode. Triggering is initiated by photons from either an unfocused laser (directly or fiber-optically coupled) or a flashlamp incident on the inside of the cup structure of the cathode. Two advantages of this triggering mechanism is that light is incident on the side of the cathode not facing the anode and hence prefires are minimized, and because a focused laser is not required there is little damage even on the part of the cathode that receives the light.

Unlike thyratrons, the BLT appears to be able to improve on several characteristics simultaneously, such as improving both the switching speed and the hold-off voltage. The BLT appears superior to most other switching devices; however, because it was developed only a few years ago very little research has been performed on this device. The purpose of this thesis is to report on the changes in switching behavior of the BLT as various parameters are changed (e.g., the gas pressure, the gas composition, the anode-cathode distance, and the diameter of the central cathode hole).

In Chapter II, secondary electron emission processes included in the model are discussed. In Chapter III, the model for the BLT is described and in Chapter IV the results from the model are discussed. Chapter V contains the conclusion.

II. SECONDARY ELECTRON EMISSION PROCESSES

Secondary electron emission processes play a major role in the operation of the BLT. Initially, the light source creates secondary photoelectrons. The photoelectrons then act as a source that generates secondary electrons and ions due to ionizations. The ions then bombard the cathode creating more secondary electrons. Secondary electrons due to the ion bombardment of the cathode play a major role in the self-sustenance of the discharge during commutation. A less important process is the emission of secondary electrons due to the electron bombardment of the anode. Thermal emission of electrons from the cathode during conduction may also be an important source of electrons[7]. We do not consider thermal emission here. The three processes, photon flux, ion bombardment, and electron bombardment were included in the model and will be discussed in detail in this chapter.

A. Photon Flux

The BLT is triggered by a flux of photons incident on the inside of the cathode cup. The flux of photons is modeled as a half-cycle sine wave. The duration of the pulse and the amplitude of the photon flux are user defined. For most applications, the duration of the pulse is very short (a few nanoseconds) and the amplitude of the flux is extremely large (about 5 MW/cm^2 at 308 nm over 13 ns). For short pulse and large amplitude the half-cycle sine wave approximation is good.

The photon flux striking the cathode causes emission of secondary

electrons[8]. This is similar to the photoelectric effect. Photons striking the cathode with energies higher than the work function of the metal will result in an emission of electrons. Photon energies less than the work function will result in heating of the cathode. For pure metals the threshold for emission is $hc/\lambda=e\phi$, where ϕ is the work function, e is the electron charge, c is light speed, and λ is the wavelength. The quantum efficiency is $2x10^{-7}$ at 308 nm and $1.2x10^{-4}$ at 222 nm for typical electrode materials[9].

Another source of photons comes about by the relaxation of excited state atoms back to ground state. If the excited state atom is not in a metastable state, then there is a high rate of relaxation of the atom back to the ground state. Relaxation to the ground state will result in an emission of a photon in any of the 4π steradians. This photon source striking the cathode will emit electrons in the same manner as do the photons from the external light source.

B. Ion Bombardment

The most important secondary electron emission process is the ion bombardment of the cathode. This process is largely responsible for the self-sustenance of the discharge. The BLT is triggered by a flux of photons, but that flux turns off after a few nanoseconds. Secondary electrons striking neutrals with high energies will cause an ionization. This process occurs most typically between the cathode and the anode within a radius slightly larger than that of the cathode hole; in this region electrons are accelerated due to high electric fields. After the ionization, electrons will continue to

drift towards the anode; the ions flowing in the same direction as the electric field will drift towards the cathode. The ions striking the cathode will result in an emission of electrons. This is one of the processes that self-sustains the discharge.

The secondary electron yield, γ, is the ratio of electrons emitted to ions striking the cathode. It depends largely on the type of cathode material and the type of gas used. In the simulation we use a cathode made of aluminum and covered with molybdenum and the various gases used are hydrogen, helium, neon, and argon. The yield also depends on the condition of the electrode. Clean surfaces will result in a higher yield. In the case of helium, there is a 30 percent decrease in yield after the first monolayer of helium covers the cathode. In this model we use $\gamma = 0.24$ for helium and hydrogen, $\gamma = 0.28$ for neon, and $\gamma = 0.12$ for argon[8].

C. Electron Bombardment

Electron bombardment of surfaces is the least important secondary emission process. High speed electrons striking the anode will result in secondary emission of electrons[8]. The yield, α, is the ratio of electrons emitted to the electrons collected by the anode. This value depends on the anode material, electron energy and gas composition. The emitted electrons initially start with a velocity in the direction of the electric field, but it does not take long before the electric field reverses the electron direction causing it to drift back towards the anode. The current contribution due to the secondary emitted electrons is negligible. In fact, the secondary

electron by itself contributes no net current to the BLT. Upon emission it contributes a negative current, and upon absorption it contributes a positive current to the BLT. The sum of these two currents can be approximated to zero. However, if the secondary emitted electron causes an ionization before returning to the anode, a net current contribution can arise. But for most practical purposes the velocity of the newly created electron will be negligible compared to the incident electron velocity. The current density and velocity is related through the relation

$$J_e = q \cdot n_e \cdot V_e$$

where J_e is the electron current density, q is the electronic charge, n_e is the electron density, and V_e is the electron velocity. Because of the direct relationship between current density and electron velocity, the majority of the current density is due to initial electrons bombarding the anode. The emitted electrons essential just "skim" on the surface of the anode.

III. DESCRIPTION OF THE BLT MODEL

In this chapter we will describe in detail the BLT geometry, the gas composition, the method used to calculate electric potential, and the methods used to calculate electron and ion densties.

A. Geometry

The BLT geometry is attractive because of its simplicity. Unlike thryatrons which require multiple grids, the BLT requires only an anode and a cathode in an inverted cup structure. The part of the cathode that faces the anode has a central hole. This hole allows transfer of electrons to the anode. Another advantage of this geometry is that there is little degradation to the side of the cathode that faces the anode. This results because the BLT is triggered by a photon source which strikes the inside of the cathode, away from the part that faces the anode.

The simulation uses a generic geometry, which is simply an inverted cup cathode with a central hole and a plane anode (Fig. 1). The user defines the anode-cathode distance, the diameter of the central hole, the height of the BLT, and the depth of the BLT. By changing various parameters of this geometry, an optimal operation point can be determined.

The most important parameter in the geometry of the BLT is the anode-cathode distance. This parameter in conjunction with the pressure of the BLT determines the hold-off voltage. The Paschen curve is a relationship which specifies the voltage required for breakdown of the gas for a given

anode-cathode distance · pressure product. A typical value for the anode-cathode distance is 3 mm, the diameter of the cathode central hole is between 2 to 10 mm, and the diameter of the BLT is typically 60 mm.

B. Gas Composition

Figure 2 shows the transport properties of the different gases which may be used in the simulation. The values of the electron transport properties for helium were obtained from a Monte Carlo simulation for electron transport[1]. Hydrogen, neon, and argon electron transport properties were obtained from electron swarm data[10]. The ion transport properties of all four gases were obtained from Reference 11. The numerical values obtained from graphs or tables were then converted into equation form for use in the simulation. A cubic polynomial regression routine available was used to fit the transport properties over specified energy intervals. The gas used in the simulation is user selectable from hydrogen, helium, neon, and argon. From the plots it is apparent that He and H_2 have higher values of ion velocity and electron and ion diffusion coefficients; however, they have lower values of ionization rate coefficients than Ne or Ar. By running the simulation with the various gases, qualities of the transport properties that result in optimal switching performance can be determined. The gases currently used in the model may not neccesarily have the values of transport properties that yield "optimal" performance, but they should be able to help in determining the values that will yield "optimal" performance. By observing the trends that result in favorable performance, "ideal" transport properties can be

determined. A mixture of gases currently used in the simulation can then be obtained so that transport properties of the gas mixture are close to "ideal." When searching for the "ideal" gas, it must be kept in mind that there is a trade-off between gas performance and gas cost.

C. Calculation of Electric Potential

Voltage is calculated using a time-dependent form of the continuity equation. The form of the equation used is

$$\nabla \cdot j = -\nabla \cdot \sigma \nabla \phi = -\frac{\partial \rho}{\partial t} \tag{1}$$

where j is the current denstiy, σ is the conductivity, ϕ is the electric potential, and ρ is the charge density.

This equation is solved using a successive over relaxation (SOR) technique. In order to obtain the desired solution many iterations must be performed. It is generally safe to iterate as many times as there are number of grid points for the first set of electric potential calculations, and about one-tenth of that for the calculation of electric potential on the updates. The goal, which is to converge to the solution as quickly as possible, can be attained much more quickly with a parameter called the SOR parameter, α. We solve for what the potential "should be" based on present values, ϕ_a. Let the correction be defined as the "actual" potential, ϕ_a, minus the old potential, ϕ_o. We can then let the updated potential, ϕ_u, equal

$$\phi_u = \phi_o + \alpha \cdot \text{"correction"} = \phi_o + \alpha \cdot (\phi_a - \phi_o) \tag{2}$$

or

$$\phi_u = (1 - \alpha) \cdot \phi_o + \alpha \cdot \phi_a \ . \tag{3}$$

By selecting a proper value for α, usually $\alpha>1$, the solution will converge more rapidly to its actual value.

Manipulation of the above continuity equation leads to the time-dependent form of Poisson's equation

$$\nabla^2\phi = \frac{1}{\sigma}\frac{\partial\rho}{\partial t} - \frac{1}{\sigma}\nabla\sigma\cdot\nabla\phi \tag{4}$$

where conductivity, σ, is the sum of the electron conductivity, σ_e, and the ion conductivity, σ_i

$$\sigma = \sigma_e + \sigma_i \tag{5}$$

and

$$\sigma_{e,i} = q\cdot n_{e,i}\cdot\mu_{e,i} \tag{6}$$

where q is the electronic charge, $n_{e,i}$ is the electron, ion density, and $\mu_{e.i}$ is the electron, ion mobility. In finite difference form, Poisson's equation can be written as

$$\frac{\partial^2\phi_{i,j}}{\partial^2 x} + \frac{\partial^2\phi_{i,j}}{\partial^2 y} = \frac{1}{\sigma_{i,j}}\cdot\frac{\partial\rho_{i,j}}{\partial t} - \frac{1}{\sigma_{i,j}}\cdot\left(\frac{\partial\sigma_{i,j}}{\partial x} + \frac{\partial\sigma_{i,j}}{\partial y}\right)\cdot\left(\frac{\partial\phi_{i,j}}{\partial x} + \frac{\partial\phi_{i,j}}{\partial y}\right) \tag{7}$$

where $\phi_{i,j}$ is the potential at grid point x_i and y_j. The second-order differential operators can be written as

$$\frac{\partial^2 a_{i,j}}{\partial x^2} = \frac{\dfrac{a_{i+1,j} - a_{i,j}}{x_{i+1} - x_i} - \dfrac{a_{i,j} - a_{i-1,j}}{x_i - x_{i-1}}}{\dfrac{x_{i+1} + x_i}{2} - \dfrac{x_i + x_{i-1}}{2}} . \tag{8}$$

The first-order differential operators can be written as

$$\frac{\partial a_{i,j}}{\partial x} = \frac{a_{i,j} - a_{i-1,j}}{x_i - x_{i-1}} . \tag{9}$$

Once the electric potential is calculated, the electric field can be calculated using

$$E = -\nabla \phi . \tag{10}$$

In finite difference form

$$(E_x)_{i,j} = -[\phi_{i+1,j+1} + \phi_{i+1,j} - (\phi_{i,j+1} + \phi_{i,j})] \cdot \frac{1}{2 \cdot (x_{i+1} - x_i)} \tag{11}$$

and

$$E_{i,j} = \sqrt{(E_x)^2_{i,j} + (E_y)^2_{i,j}} . \tag{12}$$

D. Electron and Ion Densities

The time rate of change of electron and ion densities due to convective transport are calculated using the donor cell method, which calculates the change in density by asking how many particles entered and how many particles left the cell in a set time frame having knowledge of the velocities in each adjacent cell. This velocity component term along with the ionization and diffusion terms yields the time rate of change of densities. The rate of change of electron density is

$$\frac{\partial n_e}{\partial t} = n_e \cdot N \cdot k_I + D_e \cdot \nabla^2 n_e - \nabla \cdot V_e n_e \tag{13}$$

and the rate of change of ion density is

$$\frac{\partial n_I}{\partial t} = n_e \cdot N \cdot k_I + D_I \cdot \nabla^2 n_I - \nabla \cdot V_I n_I \tag{14}$$

where $n_{e,I}$ is the electron, ion density, N is the neutral gas density, k_I is the ionization rate coefficient, $D_{e,I}$ is the electron, ion diffusion coefficient, and $V_{e,I}$ is the electron, ion velocity.

The donor cell method is particularly useful for calculating the velocity term, $\nabla \cdot V\ n$, of the rate equation. This method analyses one cell at a time. Particles in the cell under analysis with any net velocity will result in a negative contribution to $\nabla \cdot V\ n$, because particles are leaving the cell. Particles in the cell previous to the cell under analysis will make a positive contribution to $\nabla \cdot V\ n$ if the velocity in that cell is positive. Particles in

the cell following the cell under analysis will make a positive contribution to $\nabla \cdot V\, n$ if the velocity in that cell is negative, because particles are entering the cell under analysis.

$$-\nabla \cdot V_i \cdot n_i = -\,|V_i| \cdot n_i + \begin{cases} V_{i-1} \cdot n_{i-1} & V_{i-1} > 0 \\ |V_{i+1}| \cdot n_{i+1} & V_{i+1} < 0 \end{cases} . \tag{15}$$

To integrate the derivatives to obtain densities, a second-order predictor-corrector method is used. As the name implies, this method predicts a value for density, then corrects it. The predicted value at a time t is

$$n(\text{pred}) = n(\text{actual}) + \frac{\partial n}{\partial t} \cdot \Delta t \ . \tag{16}$$

At a time Δt later the predicted value of n, n(pred), is used to calculate the rate of change of n (predicted), $\frac{\partial n(\text{pred})}{\partial t}$. This value is then used to calculate the corrected value of density

$$n(\text{corrected}) = n(\text{actual}) + \left(\frac{\partial n(\text{actual})}{\partial t} + \frac{\partial n(\text{pred})}{\partial t}\right) \cdot \frac{\Delta t}{2} \tag{17}$$

The corrected value then becomes the actual value. The second-order predictor-corrector method works well in the current simulation; however, for more demanding simulations a predictor-corrector method of up to the fourth order can be used.

IV. RESULTS AND DISCUSSION

In this chapter we will describe in detail the results obtained from the BLT simulation. In Section IV.A we discuss the behavior of the electric potential and electric field, and in Sections IV.B and IV.C we discuss the behavior of the electron and ion densities, respectively. In Section IV.D we make a conjecture on how switching speed can be optimized for a given holdoff voltage.

A. Electric Potential

The equations used to calculate the electric potential and electric field were discussed in detail in Section III. C. Figure 3 shows the behavior of the electric potential before and after triggering the BLT. Penetration of the electric potential prior to triggering occurs through the central hole in the cathode. The electrons inside the cathode cup structure are drawn out by the potential penetration. The electric potential before triggering is in the vacuum configuration because the volume is free of charged particles. After triggering, ions and secondary electrons are created by various processes discussed is Chapter II. Charged particles influence the electric potential through Poisson's equation and cause deformation of the electric potential. From this excercise we see that the electric potential and charged particle density are interrelated; change in behavior of one will lead to the change in behavior of the other, and vice versa.

By observing the electric potential (Fig. 4) it is apparent that a

virtual anode builds up directly behind the cathode hole. Initially, positive potential penetrates through the cathode hole ($t < 15$ ns). Triggering, which creates negatively charged photoelectrons, causes the potential penetration to decrease. After sufficient ionizations, the ions drifting toward the cathode create a positive space charge behind the cathode hole. This positive charge causes the potential penetration to increase. The behavior of the potential through the four frames in Figure 3 verifies the presence of the virtual anode.

The electric field before and after trigger is shown in Figure 5. The relationship between the potential and field was discussed in Section III.D. By comparing this figure to the previous figure, it can be seen that the electric field is perpendicular to the electric potential at all points in space, which is the expected behavior.

B. Electron Density

The method used to calculate the electron density was discussed in detail in Section III.D. The frames in Figure 6 show the typical behavior of the electron density with respect to position at various time intervals. Initially, electrons are only at the inside surface of the inverted cup cathode, as these are the electrons due to photoemission at triggering. At a later time interval, the photoelectrons are only a small fraction of the total electron density, as electrons are created by electron avalanche between anode and cathode within a radius slightly larger than the cathode hole radius. The value of electron density is 10^7 to 10^{14} cm^{-3}. These values agree well with

experimental results. The ions created by the electron avalanche contribute to the electron density further by adding secondary electrons due to ion bombardment of the cathode as discussed is Section II.B. By the third frame, the electron density has built up to a substantial value, causing the BLT impedance to drop and current to rise. The final frame shows the switch in the conduction phase with the collapse of impedance.

Figure 7 shows the behavior of electron density in graphical form, by displaying changes in current and impedance with respect to time. Initially, the BLT behaves like an open circuit, the impedance is very large, and the current is very close to zero. During the commutation stage, the current begins to rise slowly until the electrons begin to avalanche, at which time the current rises extremely rapidly. Shortly after the electron avalanche the switch closes. The rate of current rise during electron avalanche is typically between 10^{10} to 10^{12} A/s, which agrees well with that for the experiment. This value is limited by the circuit inductance as discussed in the Introduction.

C. Ion Density

The method used to calculate ion density is discussed in detail in Section III.D. Figure 8 shows the spatial variation of ion density for several time frames. The ion density is most heavily concentrated between the electrodes within a radius not much larger than the cathode hole radius. There is a high ion density in this region because of the highly accelerated electrons in this region. High speed electrons colliding with neutrals have a

much higher probability of creating ions than do lower speed electrons, which is the reason for low ion concentration inside the cathode cup structure. Electrons between the electrodes have high velocities because of high electric fields in that region. Ion density grows somewhat proportionally to the electron density, as seen by comparing Figure 6 to Figure 8. Typical densities are between 10^5 to 10^{13} cm^{-3}.

D. Switching Time

An optimal switching time can be determined for a given holdoff voltage by convolving the pretrigger breakdown voltage relationship with the dependence of switching time on voltage. The pretrigger breakdown voltage is a function of gas compositions and electrode materials. Figure 9 shows a typical Paschen curve as a function of the product of pressure and electrode separation. The switching voltage for the BLT goes through two stages, pretriggering and after triggering. Before triggering the BLT, the breakdown curve is well described by the Paschen curve. The BLT operates on the near side of the Paschen curve, that is, on the left side of the minimum. Conventional thyratrons also operated on the near side of the Paschen curve.

After triggering the BLT, the breakdown voltage, defined as the voltage required to close the switch, depends on the pressure and electrode separation separately, not as a product. The dependence is not on the product of pressure and electrode separation because the secondary electrons deform the electric field[12]. However, the approximation that the breakdown voltage after trigger depends on the product of pressure and electrode separation is good

for our calculations.

For a given value of holdoff voltage, it can be seen from Figure 10 that the operating point must be between pd_1 and pd_2. For values of pd larger than pd_2 the BLT will break down prematurely, that is, it will break down before triggering. For values of pd smaller than pd_1 the BLT will not break down even after triggering. Both premature breakdown and no breakdown after triggering are undesirable qualities of a switching device. Therefore, the BLT must operate between pd_1 and pd_2, the operating region of the BLT for a given holdoff voltage.

Figure 11 is a plot of the switching time as a function of pressure and electrode separation. Switching time is the time interval between triggering and switch closure; switching time is commonly known as the anode delay time. In order to satisfy the operating region conditions from the last paragraph, operation must take place between the curves pd_1 and pd_2 of the switching time plots shown in Figure 12. By considering the switching time plot, an optimal switching speed can be determined given the constraint that operation must be between pd_1 and pd_2, $pd_1 < pd < pd_2$. The optimal switching speed will yield the optimal pressure, p_{opt}, or a range of optimal pressures, and optimal electrode separation, d_{opt}, or a range of optimal electrode separations.

E. Nonswitching Behavior

Whether the switch closes or not depends largely on the gas pressure and the electrode separation to a lesser degree. The electric potential, electron density, and ion density behave differently when switch closure does not

occur. Compare the electric potential when switch closure occurs (Fig. 4) to when switch closure does not occur (Fig. 13). Initially, the behavior is quite similar; however, at later times Figure 4 and Figure 13 differ dramatically. When switch closure does not occur, the electric potential does not penetrate back into the cathode cup. In other words, a virtual anode does not form when the switch does not close.

The electron density (Fig. 14) behaves completely differently when switch closure does not occur than when the switch does close (Fig. 6). Notice that the electron density is a minimum in the high field region (Fig. 14). Ions behave similarly to electrons when the switch does not close (Fig. 15).

Figure 16 shows the behavior of current vs. time when switch closure does not occur. Initially, this plot is simliar to Figure 7, which is a plot of current vs. time when the switch does close. However, in Figure 16 the current reaches a maximum, then begins to decrease rapidly. The current decreases because the secondary electron emission processes are not strong enough to sustain the discharge. The result is a decrease in electron density and, therefore, a decrease in current.

The sequence of events when switch closure does not occur is: (1) Low gas pressure results in low neutral gas density; therefore, electrons have fewer partners to collide with, resulting in fewer ions; (2) Because the ion density is low, a net positive space charge inside the cathode cup is very small; (3) Because of the lack of positive space charge, the potential penetration after trigger is minimal; therefore, a virtual anode does not form; (4) Because of the absence of the virtual anode, there are no gradients

in the potential within the cathode cup; (5) Because of the lack of the potential gradient, the electrons do not have any tendency to drift out of the cathode cup. This results in nonclosure of the switch.

V. CONCLUSIONS

The results obtained from the BLT simulation agree well with experimental data obtained by Professor Martin Gundersen at the University of Southern California. The simulation begins with the triggering of the BLT and ends when switch closure occurs. After triggering the BLT, several secondary electron emission processes sustain the discharge. The most important secondary emission processes are ion bombardment of the cathode and ionizations in the high field region. After closure, we expect that other emission processes, such as thermal emission due to cathode heating, will be necessary to obtain higher currents.

By referring to the results of Figure 12 it can be seen that higher gas pressures result in shorter closure times. This occurs because a higher neutral gas density gives the electrons more partners to collide with, resulting in a higher probability of ionization, and the higher collision frequency overshadows the reduction in E/N. Another trend that can be observed from Figure 12 is that switch closure time decreases with increasing electrode separation. This occurs because larger electrode separation gives the electrons more chances to create electron-ion pairs. The obvious question at this point is "why not operate at high pressures and large electrode separations?" At high gas pressures and/or large electrode separations, we will be operating near the minimum of the Paschen curve, which means that the holdoff voltage will be low. We see that the trade-off between holdoff voltage and switch closure time is inherent in the BLT; however, the trade-off does not seem to be as limited as in conventional thyratrons.

The dependence of gas pressure and incident photon flux on switch closure time is also very important. Gas pressure appears to determine whether or not the switch will close; photon flux appears to determine the speed of switch closure. For instance, if the gas pressure is high, the switch will eventually close even if the photon flux is very small. If the gas pressure is low, the switch will not close even for a very high photon flux (within reason). Therefore, if the pressure is in a range that will cause switch closure, a higher photon flux will result in a shorter closure time.

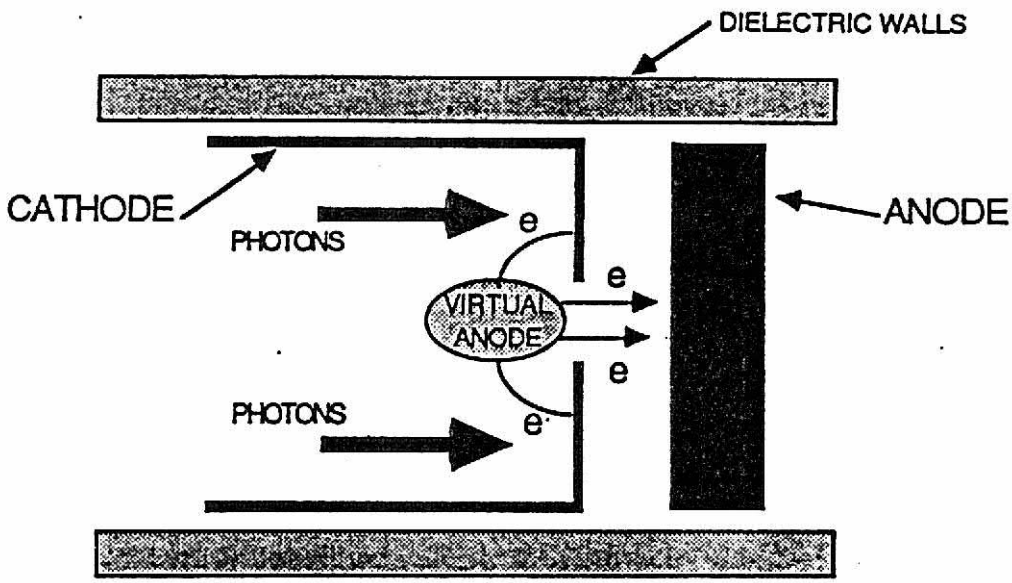

Fig. 1. The BLT geometry. Inverted cup cathode structure with central hole, and plane anode. Light source striking inside the cathode cup.

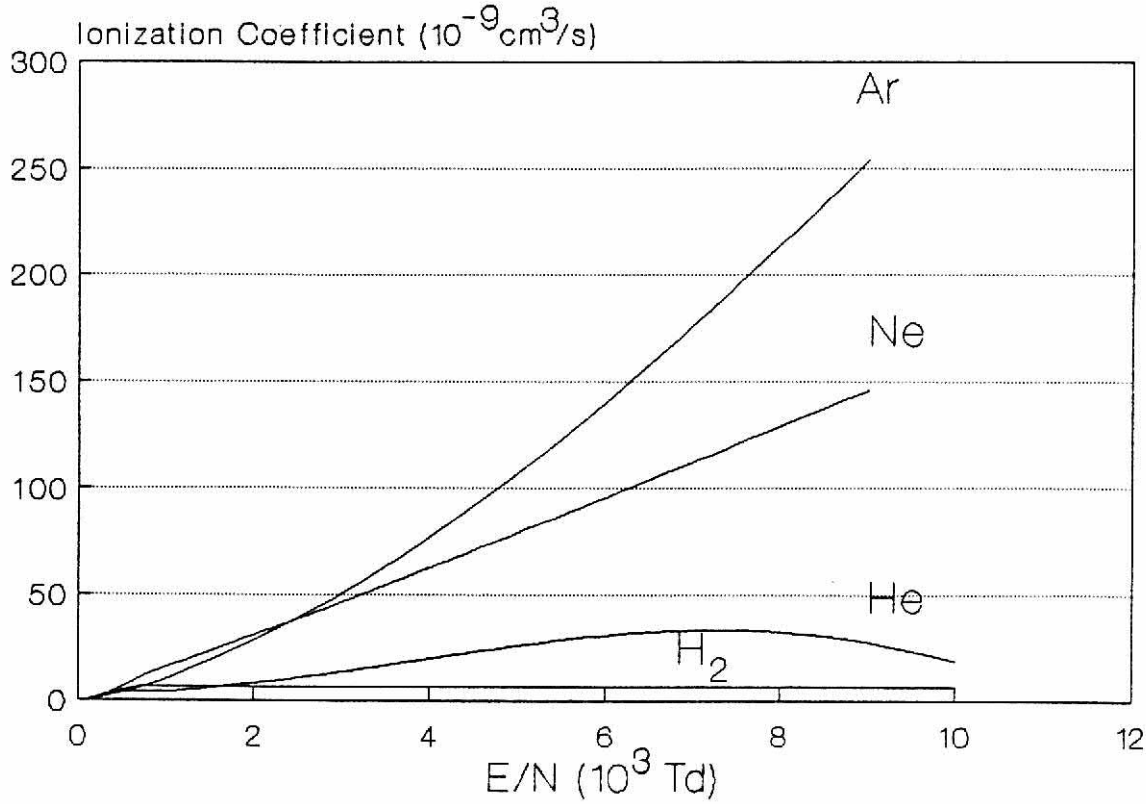

Fig. 2(a)

Fig. 2. Various gases and their transport properties. Gases available in the simulation are hydrogen, helium, neon, and argon. Compare (a) ionization rate coefficient, (b) electron velocity, (c) ion velocity, (d) electron diffusion coefficient, and (e) ion diffusion coefficient for the various gases available in the simulation.

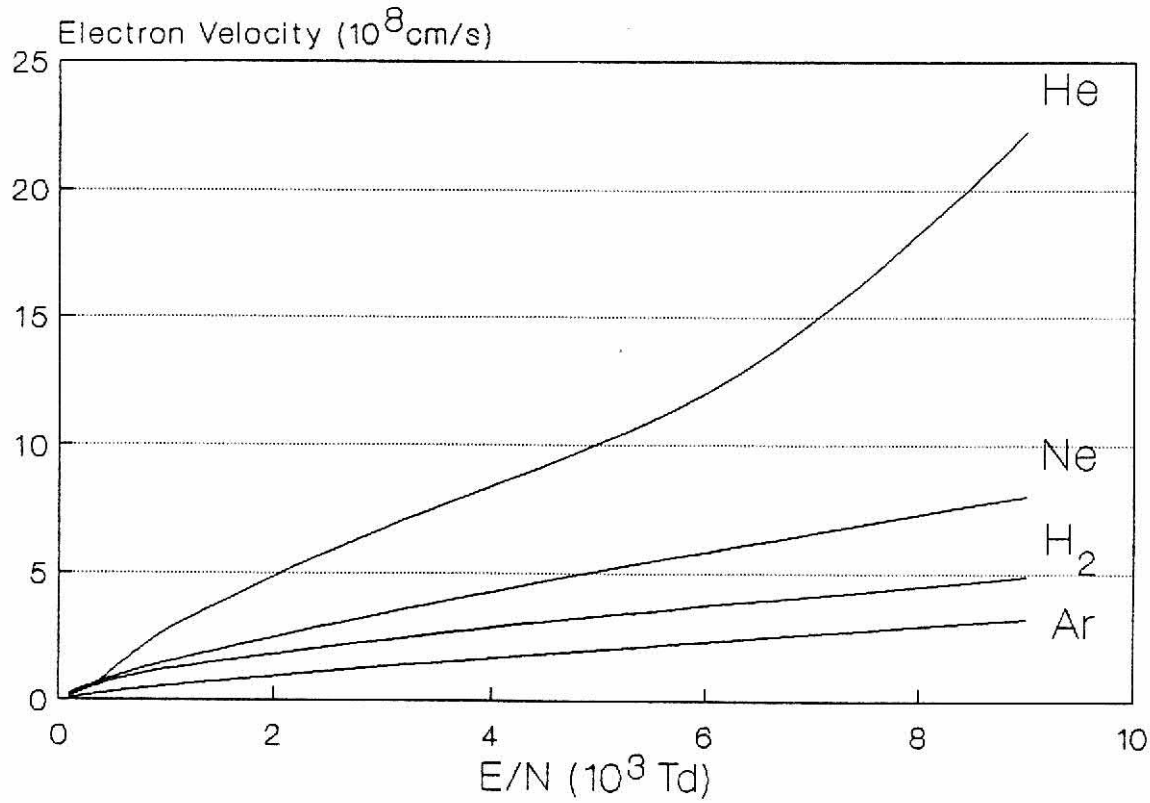

Fig. 2(b). Electron velocity

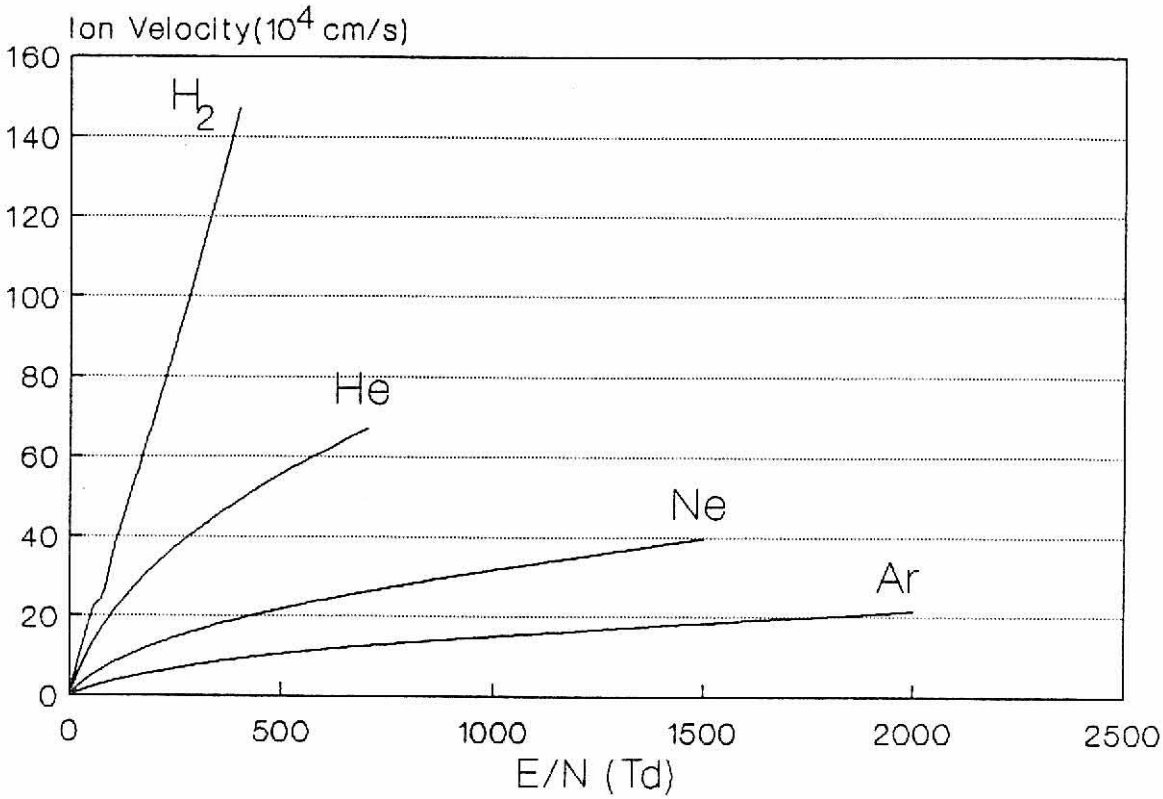

Fig. 2(c). Ion velocity

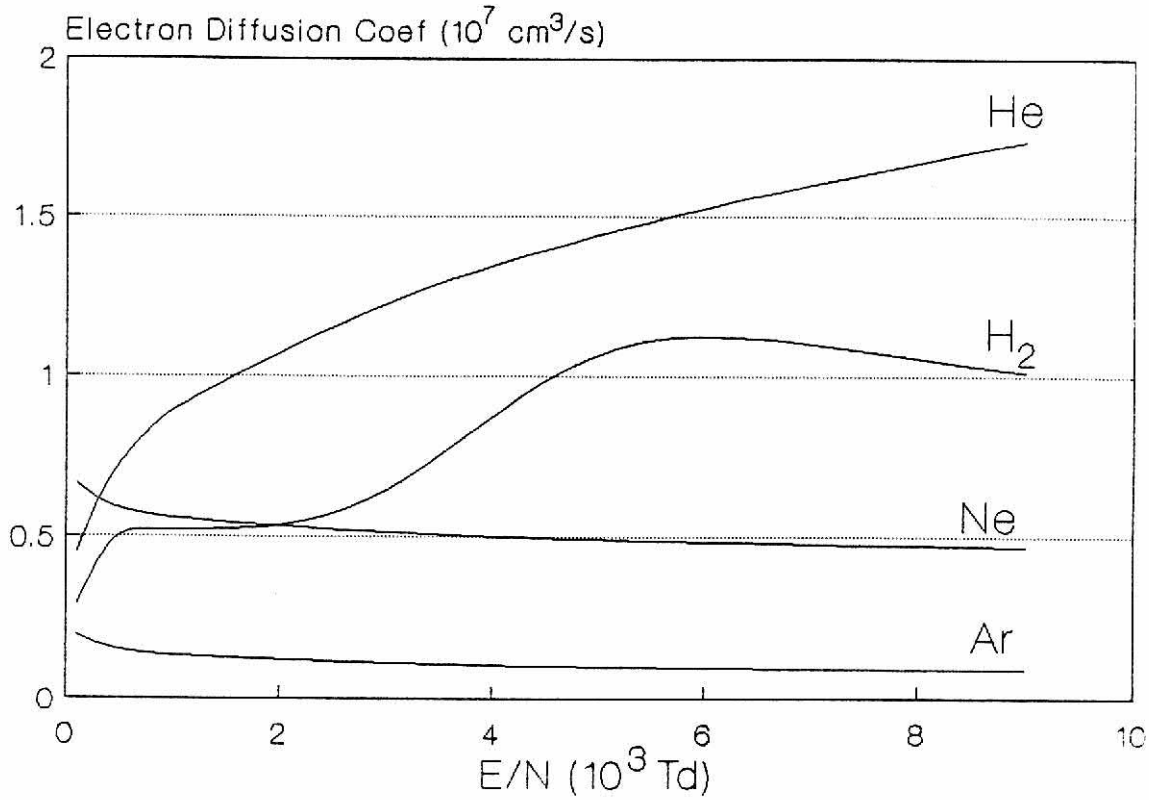

Fig. 2(d). Electron diffusion coefficient

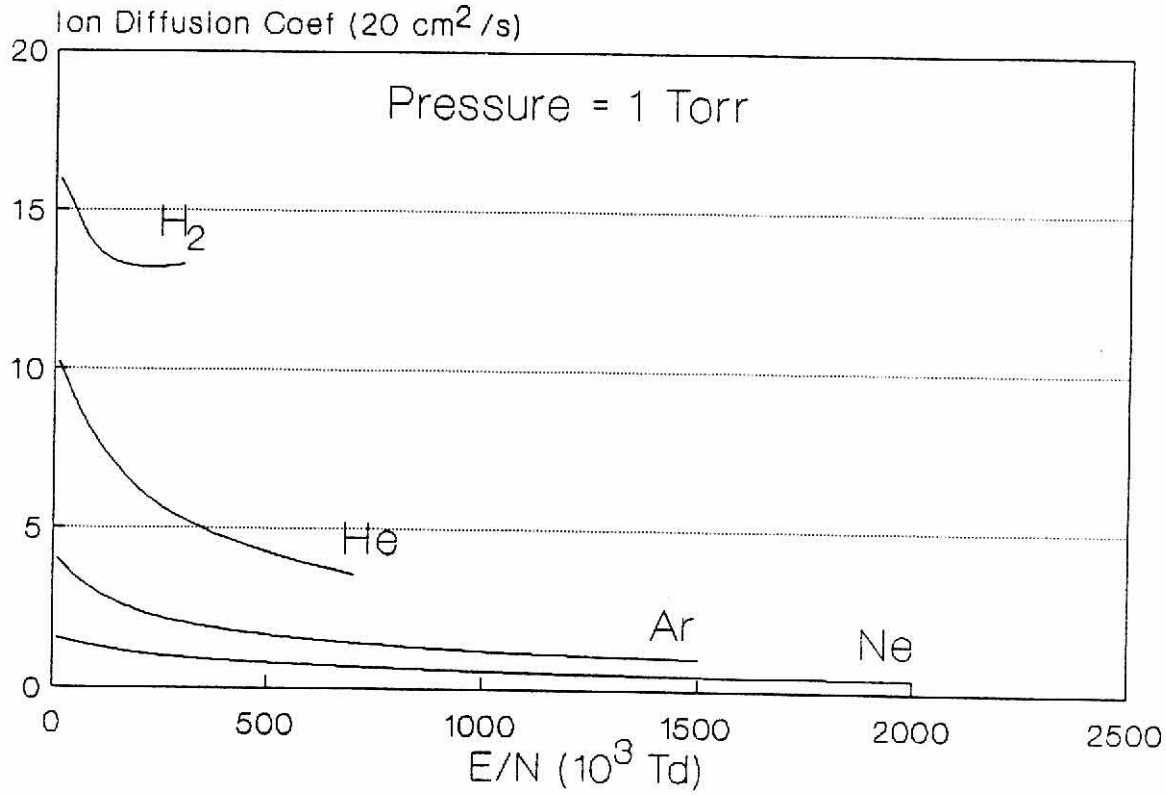

Fig. 2(e). Ion diffusion coefficient

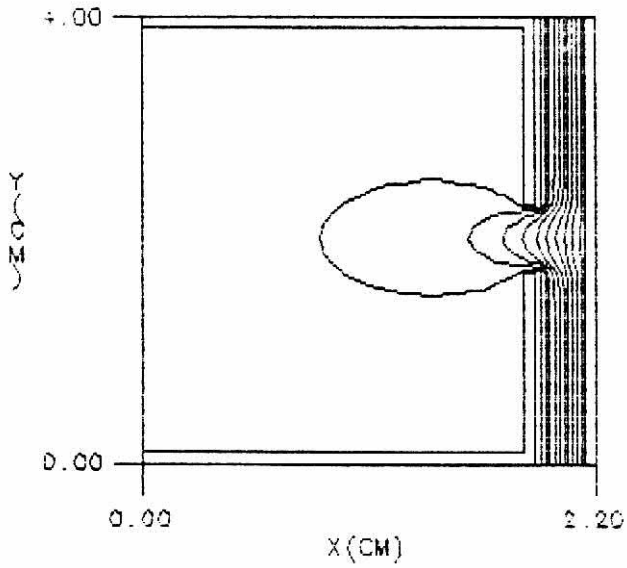

Fig. 3(a)

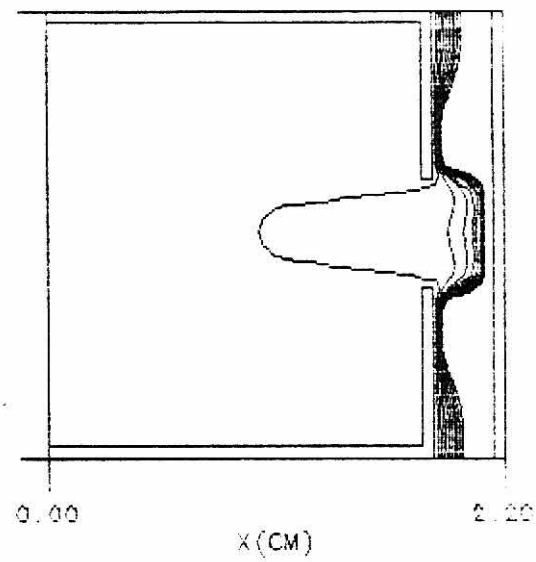

Fig. 3(b)

Fig. 3. Electric potential (a) before and (b) after trigger. Before trigger, the potential is in the vacuum configuration because the volume is free of charged particles. After trigger, the charged particles deform the potential.

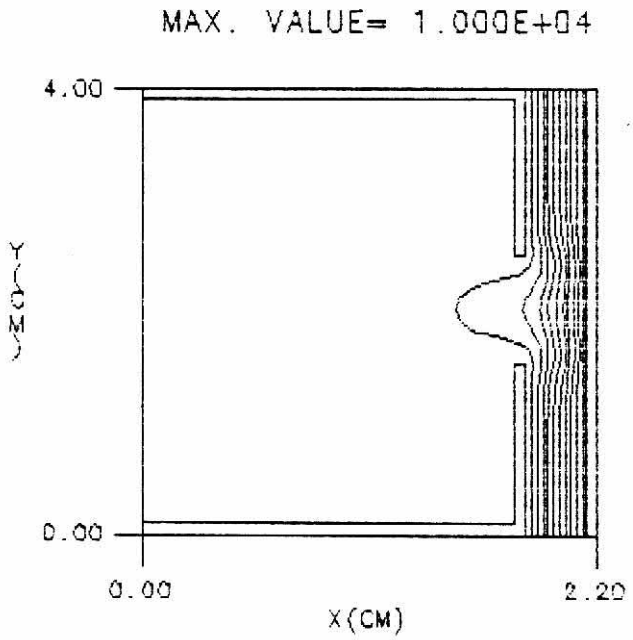

t = 2 ns

Fig. 4(a)

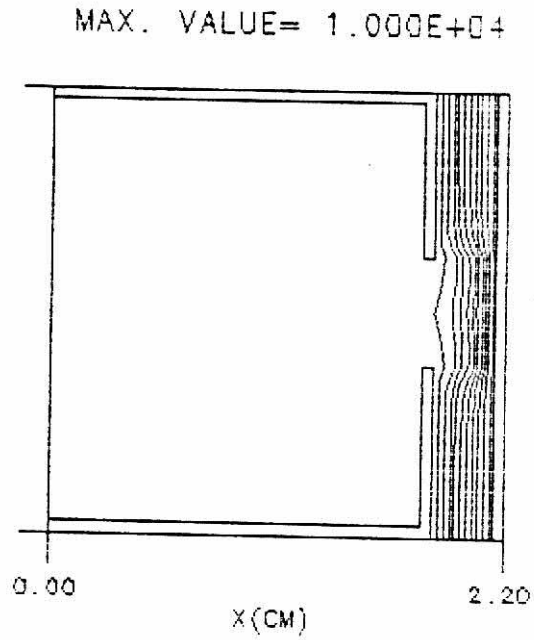

t = 3 ns

Fig. 4(b)

Fig. 4. Changes in behavior of the electric potential caused by the virtual anode. Before trigger, the potential is shown in Figure 3(a). Shortly after trigger, the potential penetration decreases because of the negatively charged photoelectrons, as shown in (a) and (b). The potential penetration "reappears" because of the buildup of ions (c) and (d).

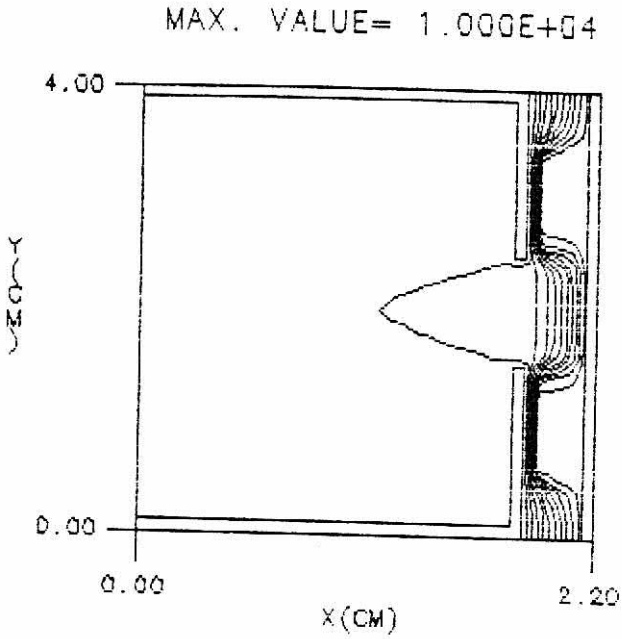

t = 12 ns

Fig. 4(c)

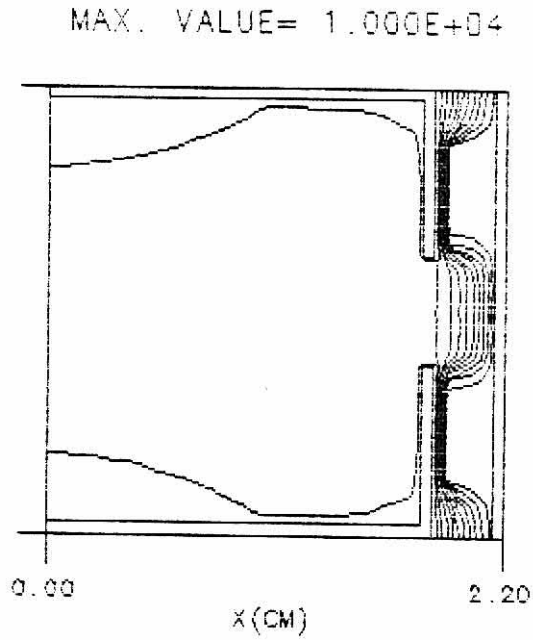

t = 13 ns

Fig. 4(d)

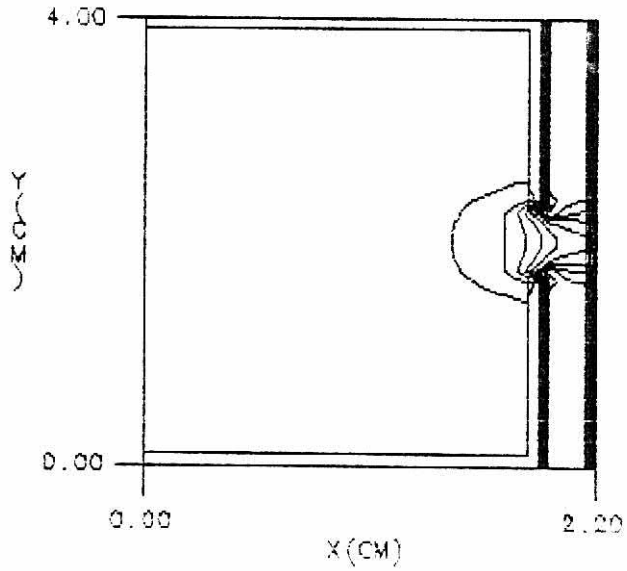

Fig. 5(a)

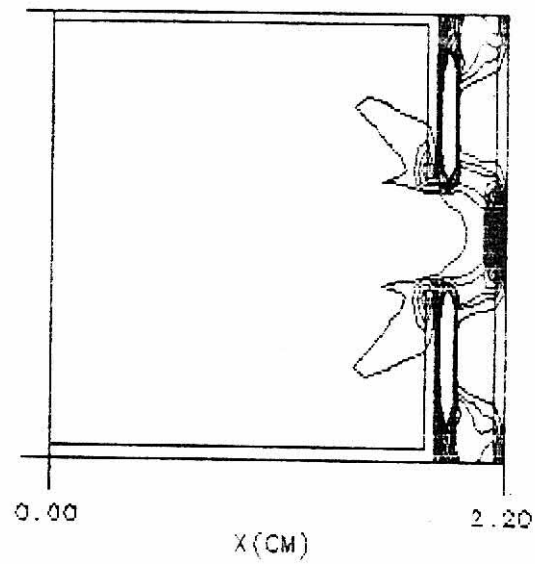

Fig. 5(b)

Fig. 5. Electric field before trigger (a), and after trigger (b). The electric field behaves as expected, perpendicular to the electric potential at all points in space.

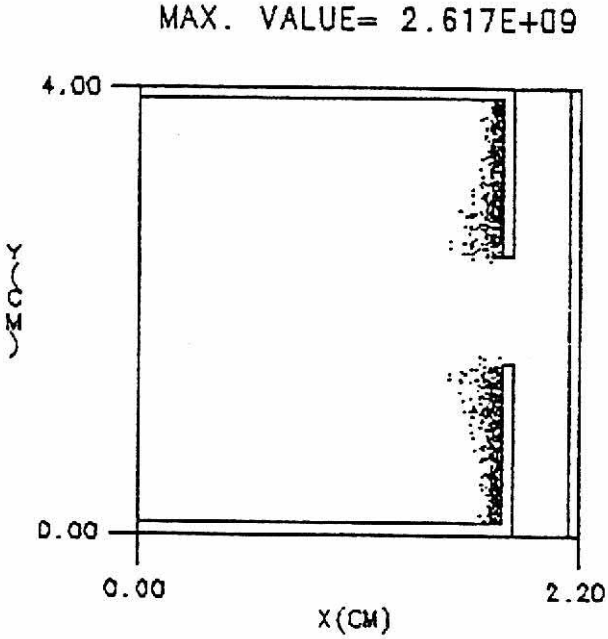

t = 1 ns

Fig. 6(a)

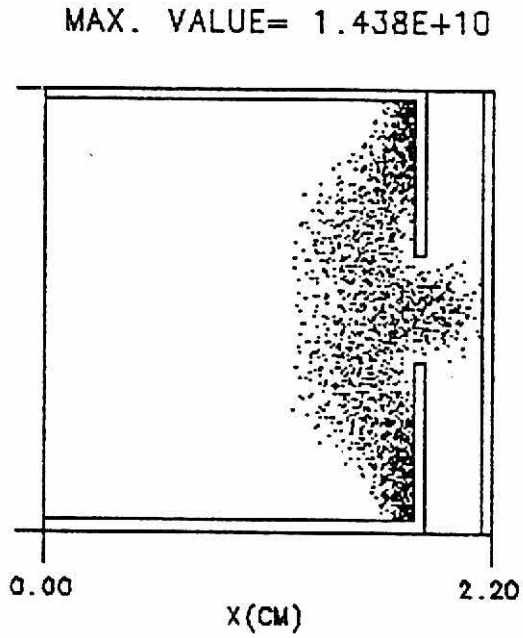

t = 40 ns

Fig. 6(b)

Fig. 6. Electron density for several time frames. Initially, electrons are only at the inside surface of the cathode cup (a). The potential penetration draws the electrons out (b), (c). At switch closure the electron density increases to approximately 10^{14} cm^{-3} (d).

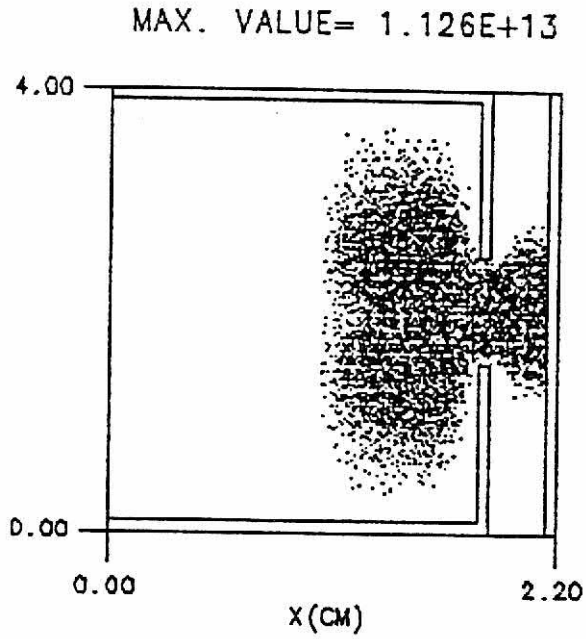

t = 80 ns

Fig. 6(c)

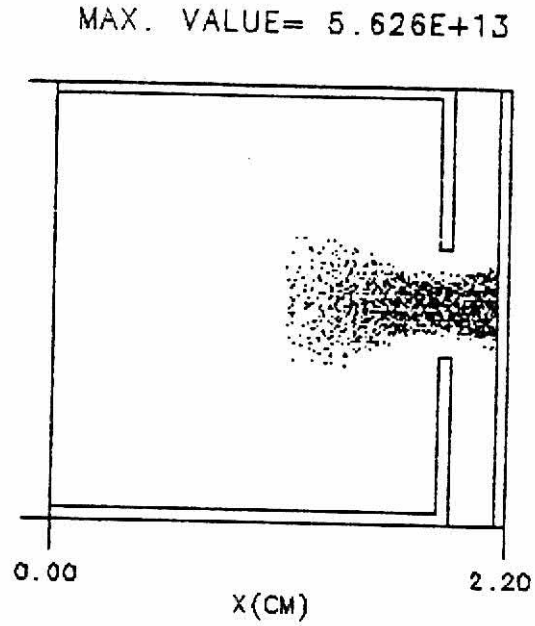

t = 130 ns

Fig. 6(d)

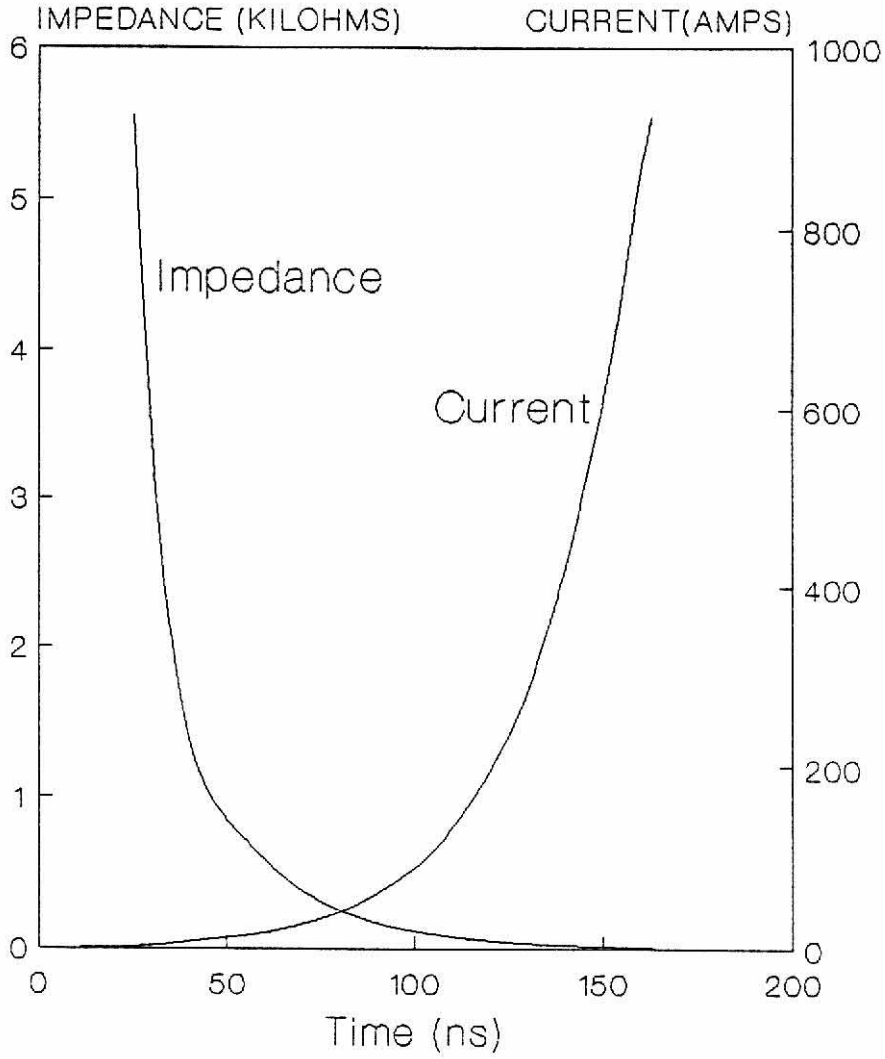

Fig. 7(a)

Fig. 7. (a) Collapse of impedance and rise of current as a function of time. (b) Dependence of switching speed on photon flux.

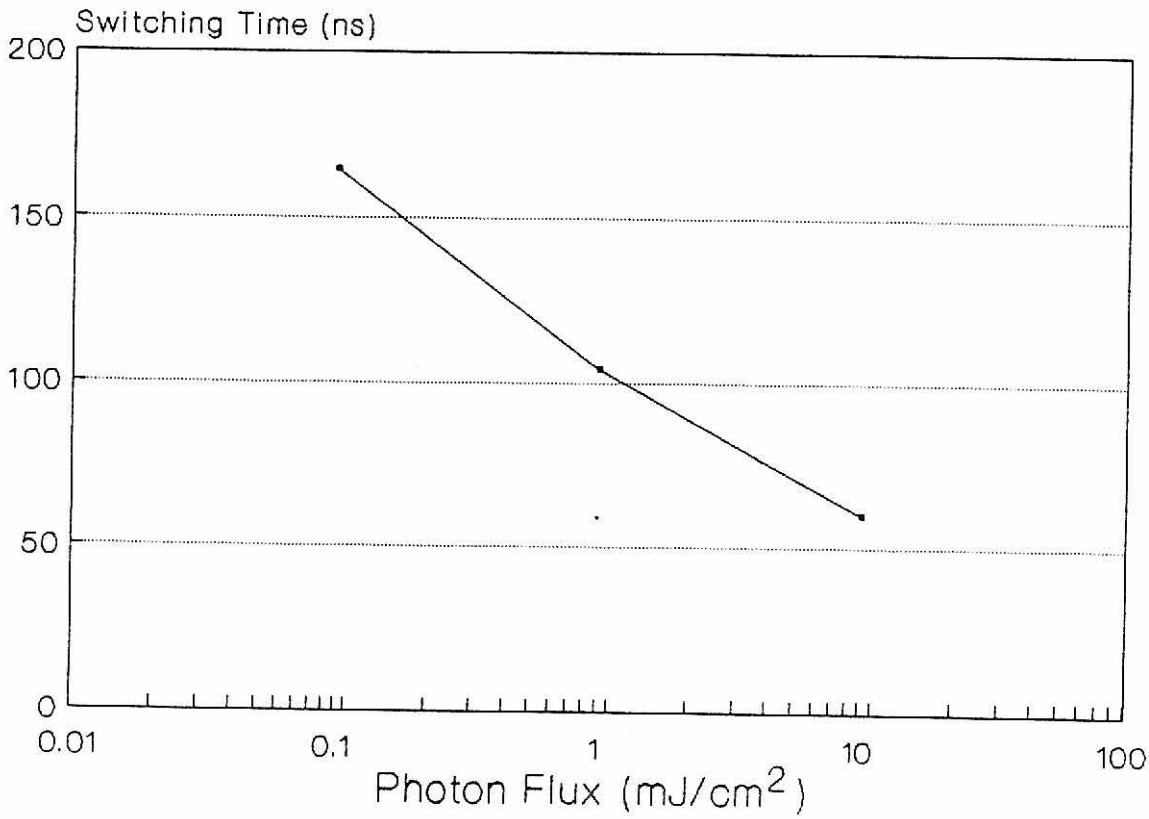
Switching Time (ns)
200
150
100
50
0
0.01
0.1
1
10
100
Photon Flux (mJ/cm2)

Fig. 7(b)

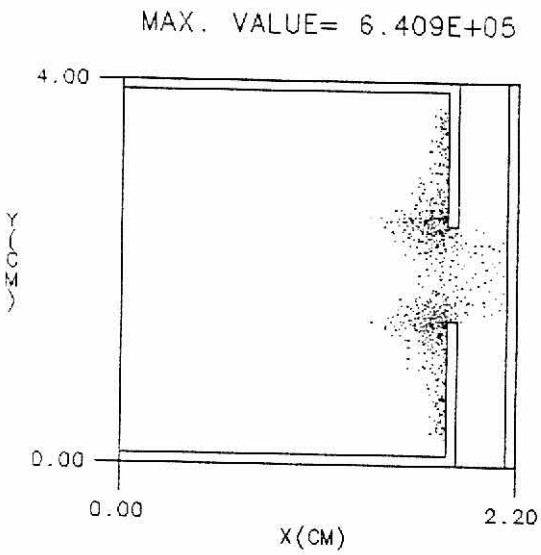

t = 1 ns

Fig. 8(a)

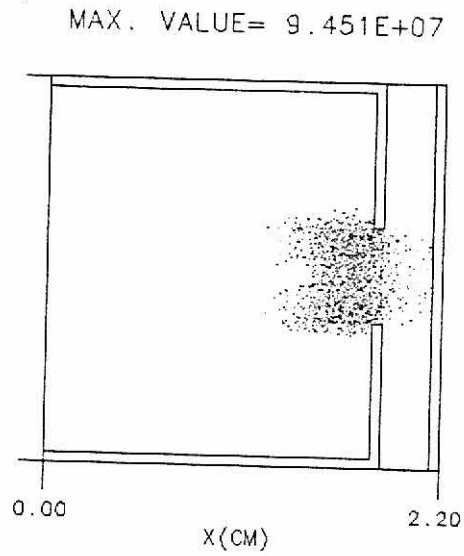

t = 13 ns

Fig. 8(b)

Fig. 8. Ion density for several time frames, (a) at t = 1 ns, (b) at t = 13 ns, (c) at t = 80 ns, and (d) at t = 130 ns. Ions are heavily concentrated between the electrodes within a radius slightly larger than that of the cathode hole.

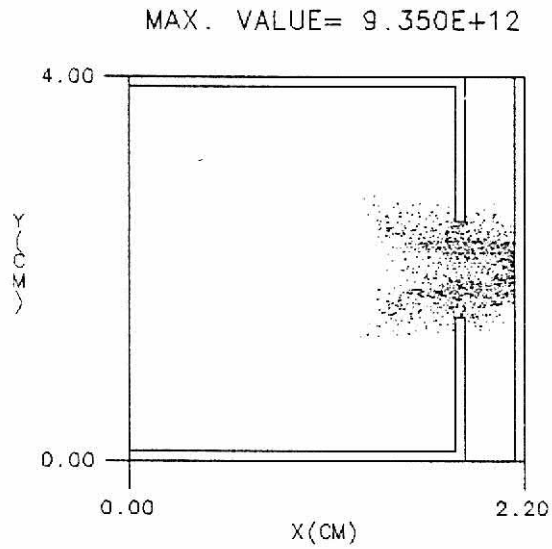

t = 80 ns

Fig. 8(c)

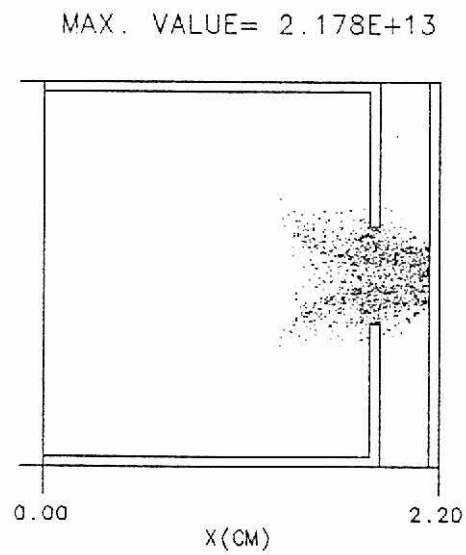

t = 130 ns

Fig. 8(d)

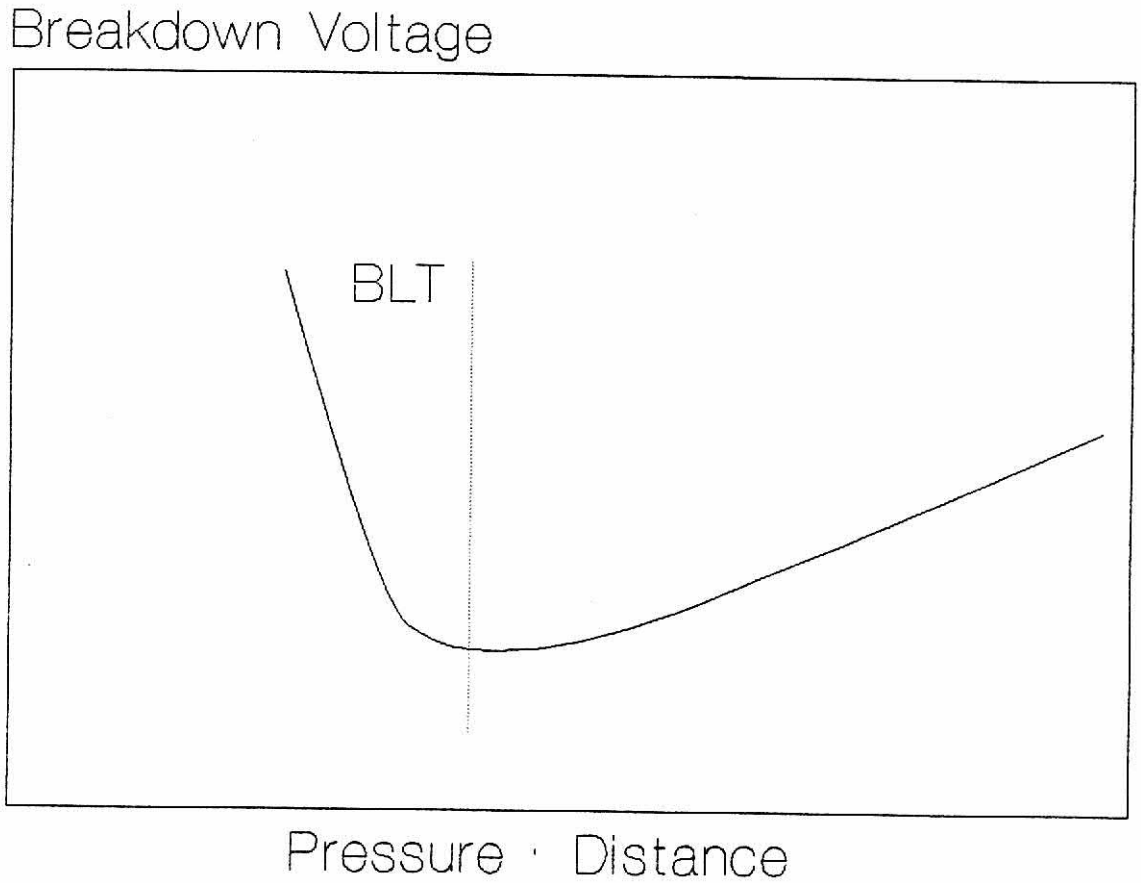

Fig. 9. Typical Paschen curve. Paschen curve shows the voltage required to create an electron avalanche as a function of the product of pressure and electrode separation. Note that the BLT operates on the near side of the Paschen curve.

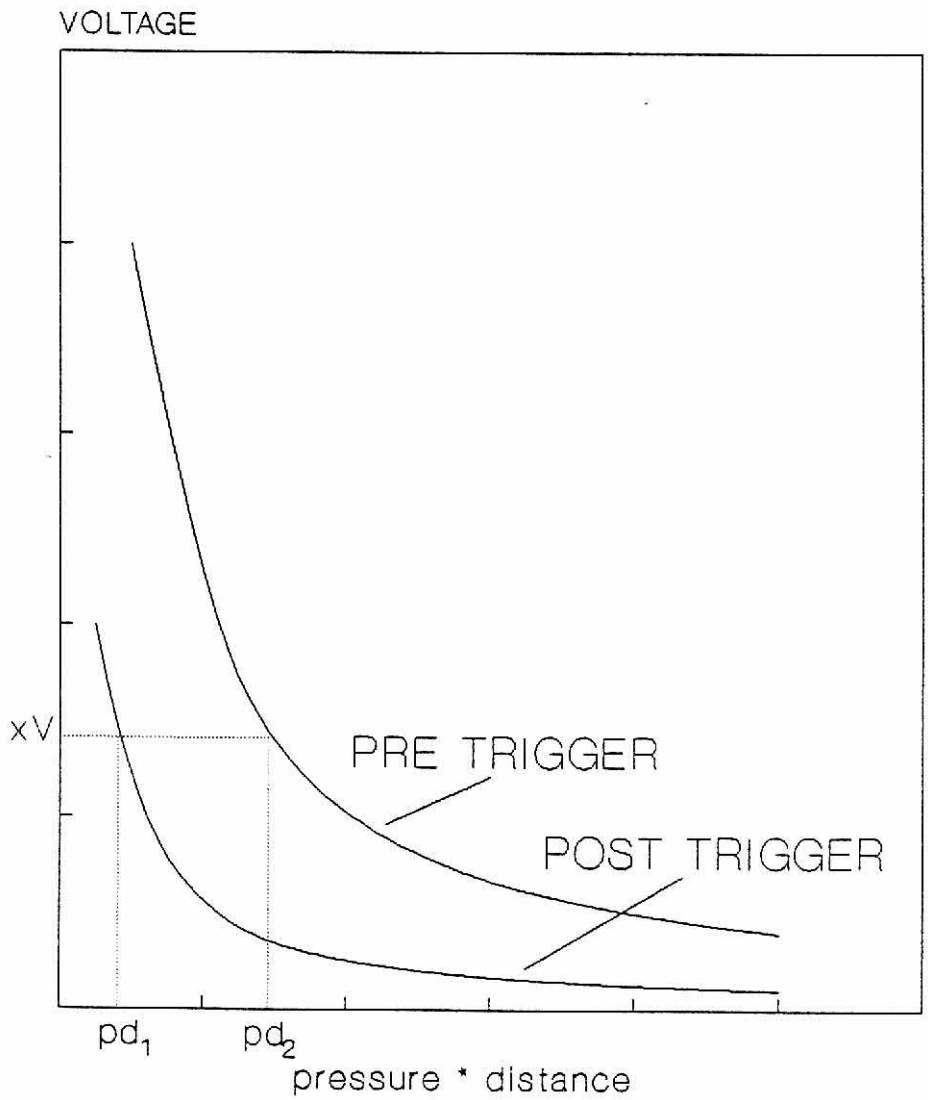

Fig. 10. Voltage breakdown curve before and after trigger. For a given holdoff voltage, xV, the operating region is between pd_1 and pd_2.

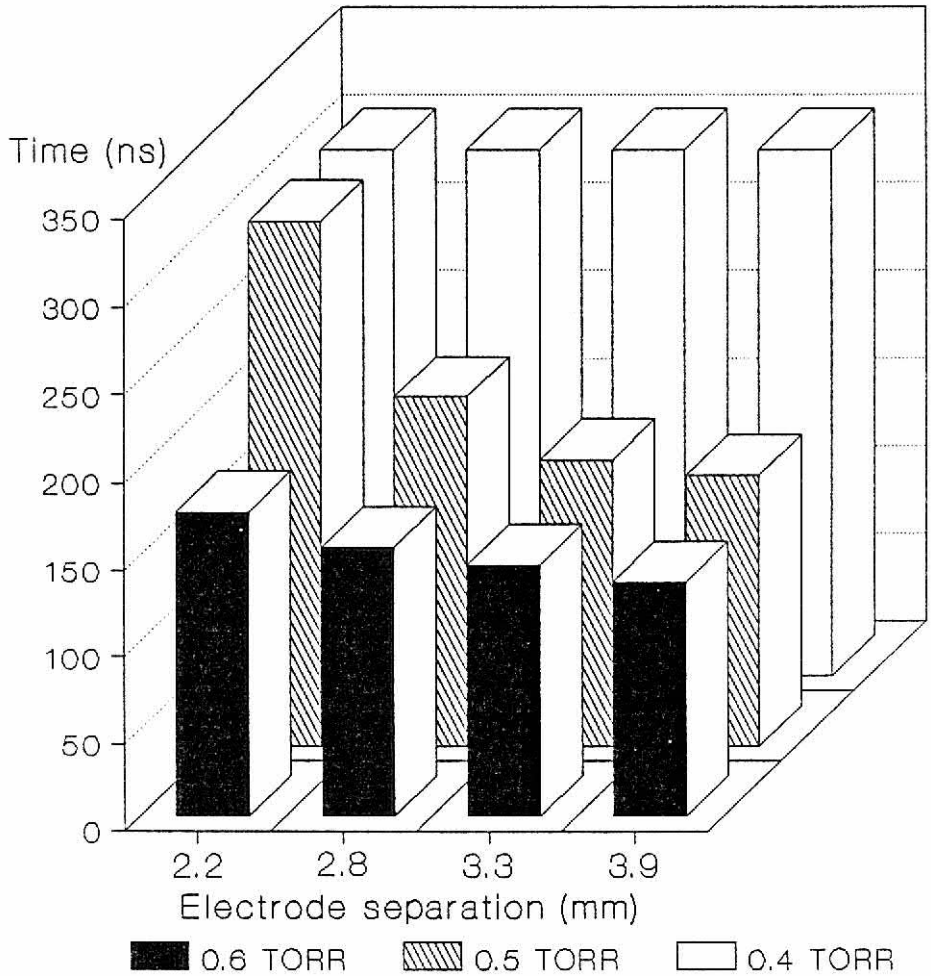

Fig. 11. Switching time as a function of pressure and distance.

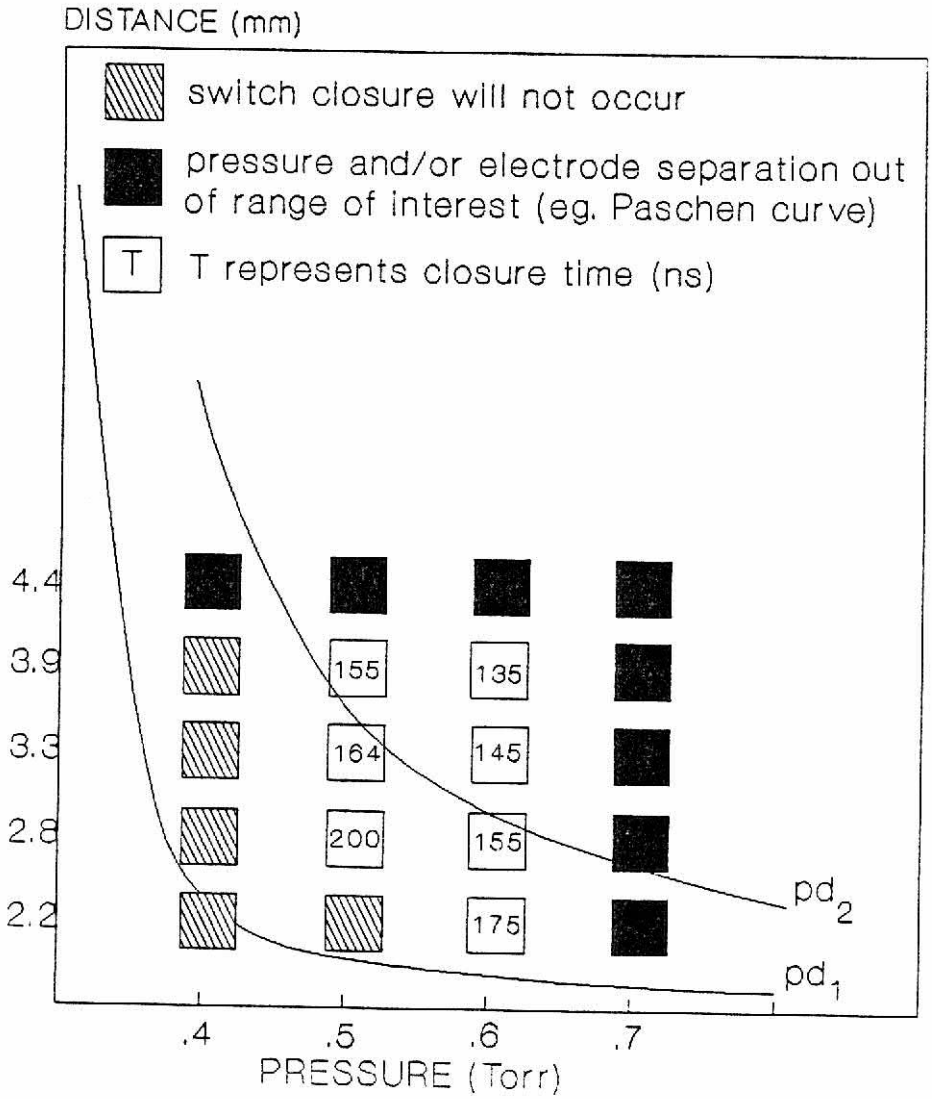

Fig. 12. Optimal operating point. Obtain operating region from Fig. 10 and superimpose the operating region on the switching time plot. Determine optimal operating point by finding the fastest switching speed within the operating region.

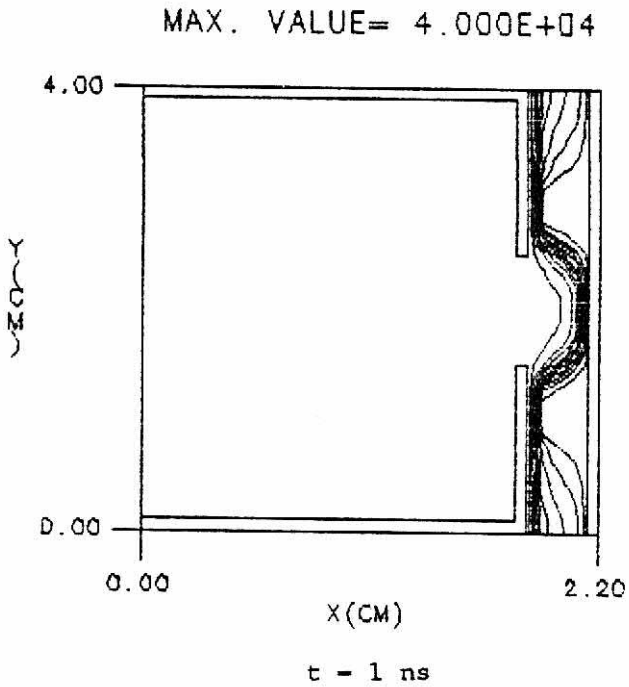

Fig. 13(a)

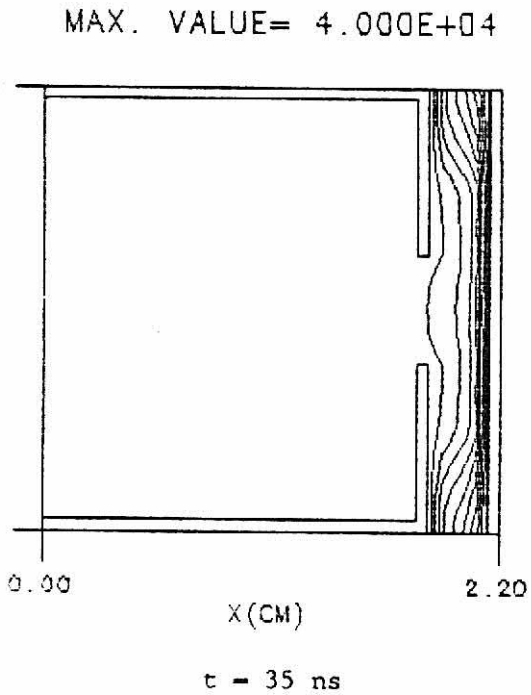

Fig. 13(b)

Fig. 13. Nonclosure behavior of electric potential for several time frames, (a) at t = 1 ns, (b) at t = 35 ns, (c) at t = 70 ns, and (d) at t = 105 ns. Notice that the virtual anode does not exist when the switch does not close.

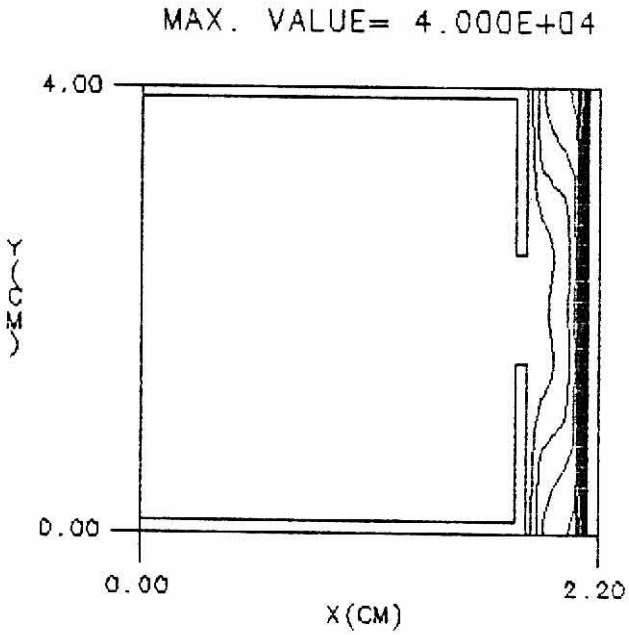

t = 70 ns

Fig. 13(c)

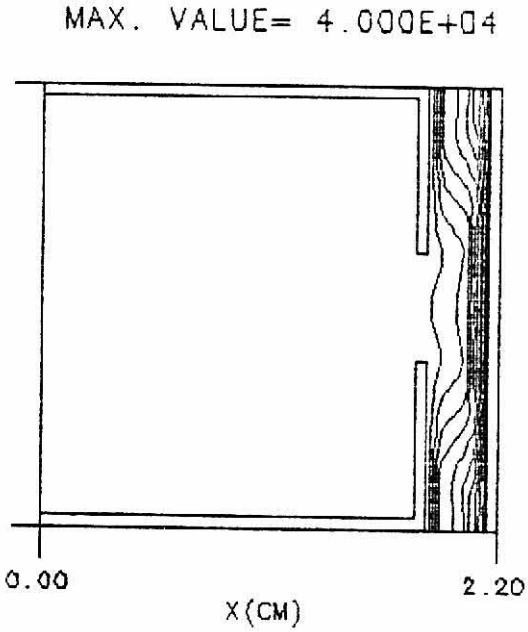

t = 105 ns

Fig. 13(d)

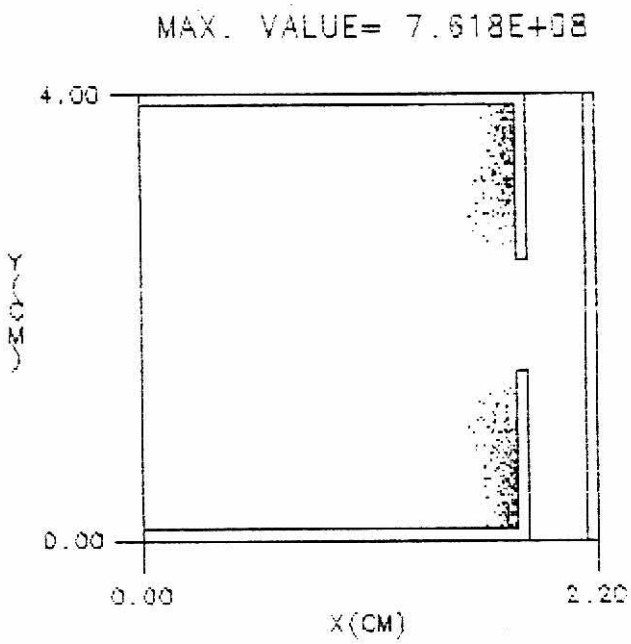

t = 1 ns

Fig. 14(a)

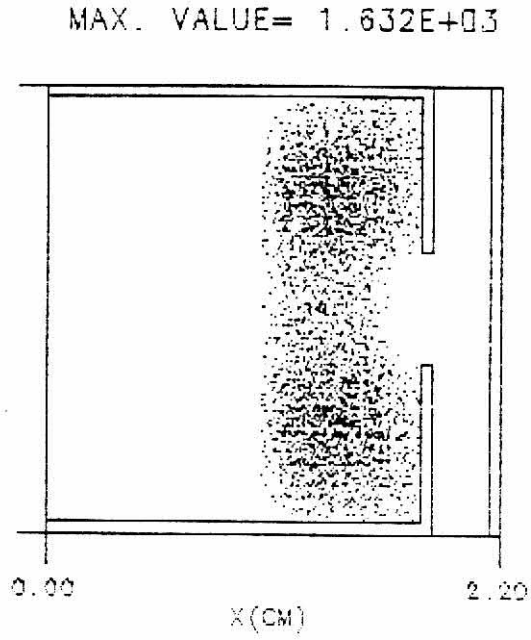

t = 35 ns

Fig. 14(b)

Fig. 14. Nonclosure behavior of electron density for several time frames, (a) at t = 1 ns, (b) at t = 35 ns, (c) at t = 70 ns, and (d) at t = 105 ns. Electron density is very low in the high field region. The time frames show a decrease in electron density with respect to time.

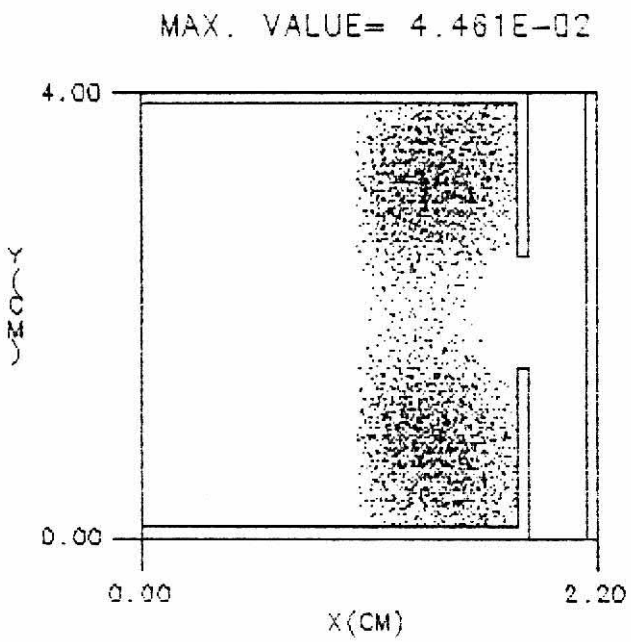

t = 70 ns

Fig. 14(c)

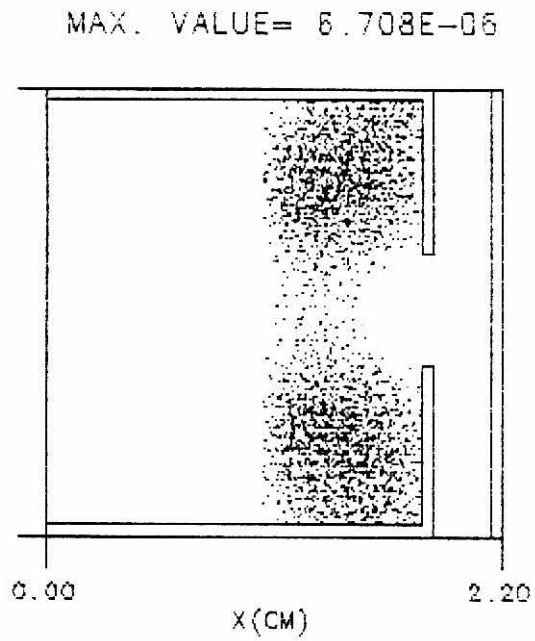

t = 105 ns

Fig. 14(d)

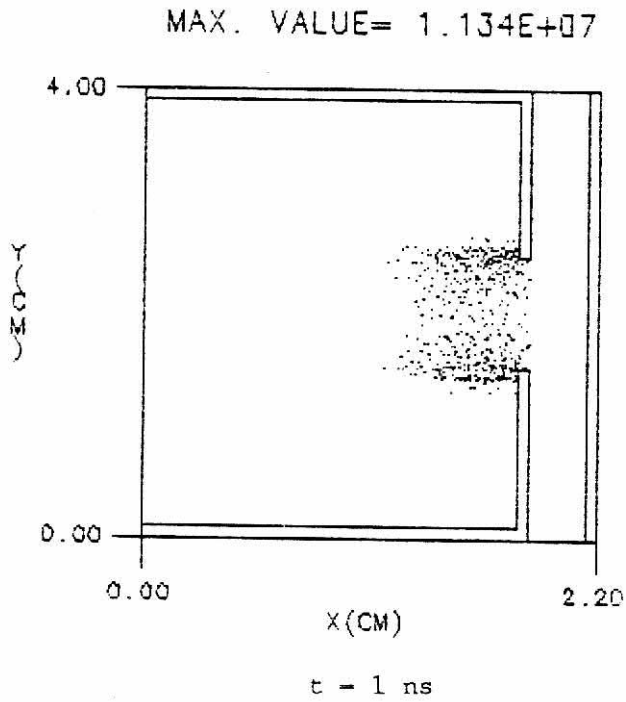

Fig. 15(a)

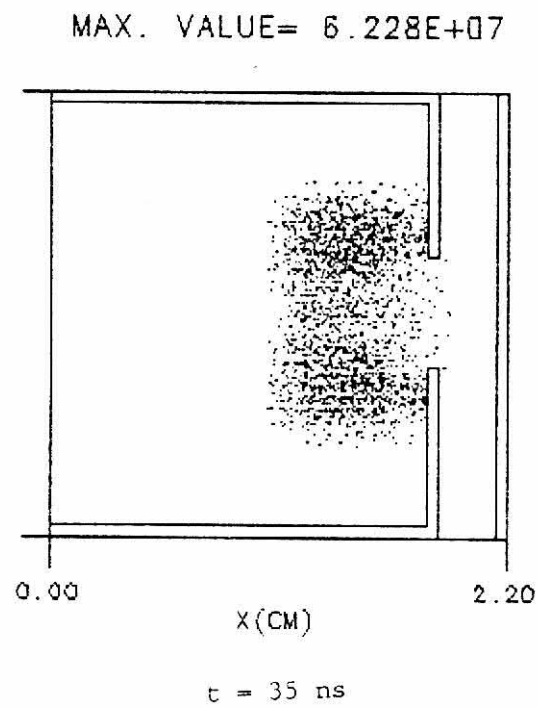

Fig. 15(b)

Fig. 15. Nonclosure behavior of ion density for several time frames, (a) at t = 1 ns, (b) at t = 35 ns, (c) at t = 70 ns, and (d) at t = 105 ns. Unlike Figure 8, the ion density is very low between the electrodes.

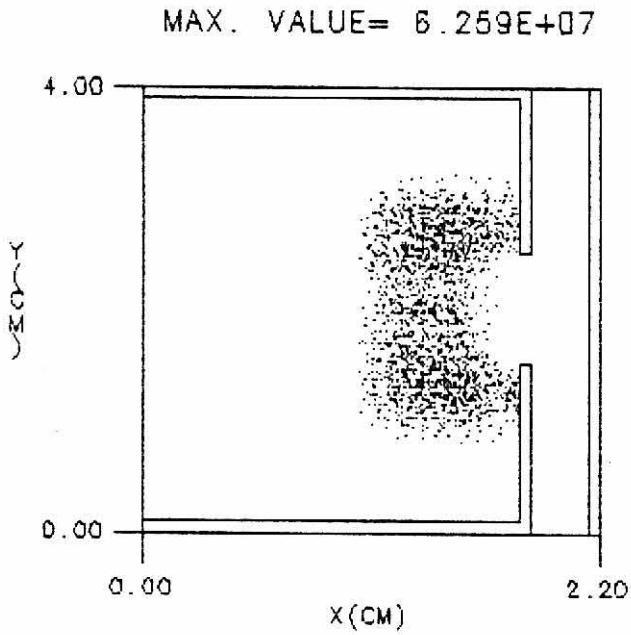

t = 70 ns

Fig. 15(c)

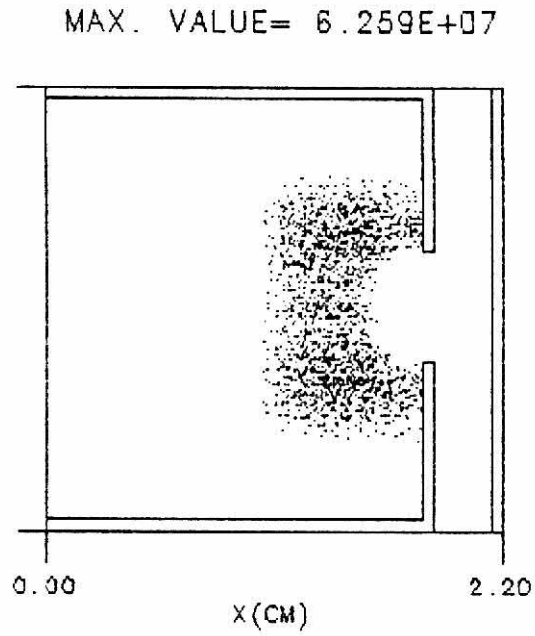

t = 105 ns

Fig. 15(d)

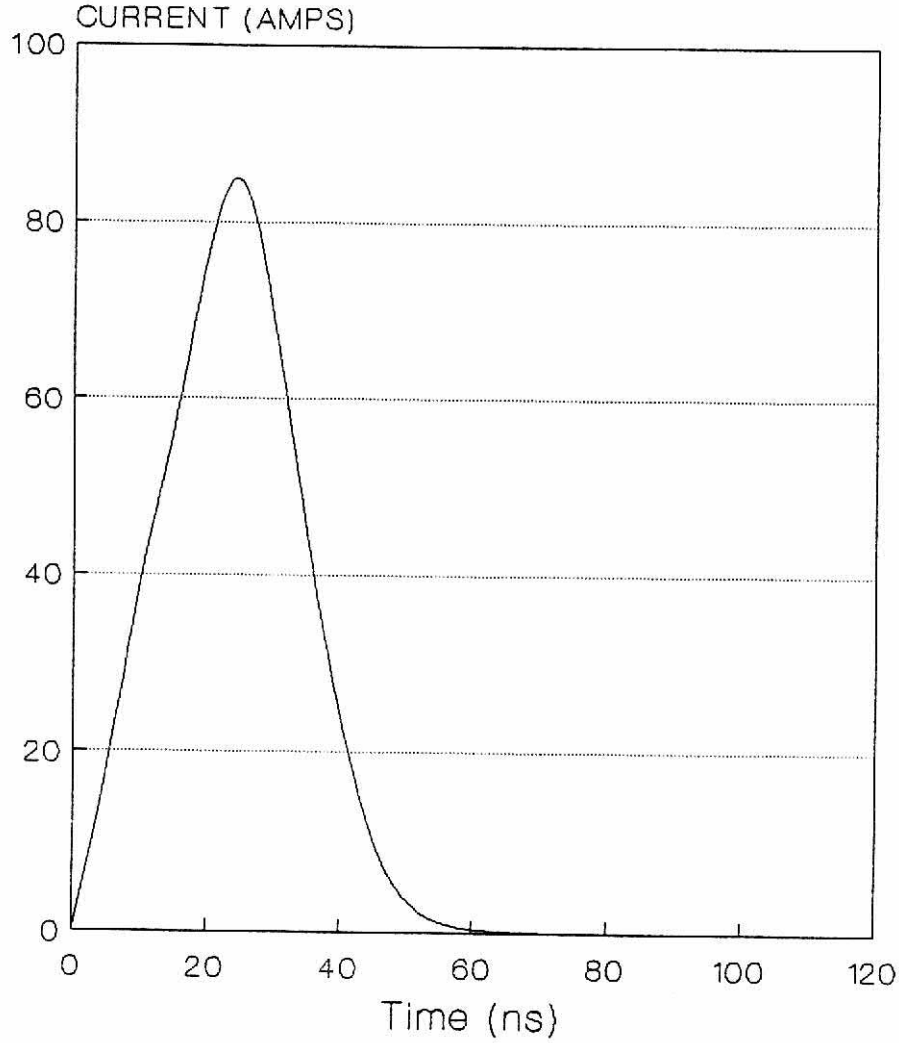

Fig. 16. Nonclosure behavior of current vs. time. Initially, current begins to rise; however, at later times it reaches a maxima, then falls off rapidly.

REFERENCES

[1] G. Kirkman and M. Gundersen, Appl. Phys. Lett. **49** (9), 494 (1986).

[2] G. Kirkman, W, Hartmann, and M. Gundersen, Appl. Phys. Lett. **52** (8), 613 (1988).

[3] K. Frank, E. Boggasch, J. Christiansen, A. Goertler, W. Hartmann, C. Kozlik, G. Kirkman, C. Braun, V. Dominic, M. Gundersen, and H. Riege, "High power hollow electrode thyratron-type switches," in Proceedings of the IEEE Pulsed Power Conferences, June 1987.

[4] G. Mechtersheimer, R. Kohler, T. Lasser, and R. Meyer, J. Phys. E: Sci. Instrum. **19**, 466, (1986).

[5] D. Bloess, I. Kamber, H. Riege, G. Bittner, V. Brueckner, J. Christiansen, K. Frank, W. Hartmann, N. Lieser, C. Scheltheiss, R. Seeboeck, and W. Seudtner, Nucl. Instrum. Meth. **205**, 173, (1983).

[6] M. Kushner, J. Appl. Phys. **61** (8), 2784 (1987).

[7] W. Hartmann and M. Gundersen, "Origins of anomalous emission in superdense glow discharge," submitted to IEEE Trans. Electron Devices.

[8] B. Chapman, *Glow-Discharge-Processes* (John Wiley & Sons, New York, 1980), pp. 82-95.

[9] Professor Martin Gundersens notes, University of Southern California, unpublished.

[10] J. Dutton, J. Phys. Chem. Ref. Data, **4** (3), (1975).

[11] H. Ellis, R. Pai, E. McDaniel, E. Mason, and L. Viehland, Atomic Data and Nuclear Data Tables, vol. 17, no. 3, 177, (1976).

[12] A Von Engel, *Electric Plasmas: Their nature and uses* (International Publications Services, New York, 1983), pp. 123-127.